AIAA JOURNAL
Vol. 40, No. 6, June 2002

Mean Flow Development in Dual-Stream Compressible Jets

Erina Murakami* and Dimitri Papamoschou†
University of California, Irvine, Irvine, California 92697-3975

We present experimental results on the mean flow development and potential core lengths of single- and dual-stream compressible air jets. The research is relevant to noise emission, thermal signature, and combustion in high-speed turbulent jets. The primary flow was set at Mach number 1.5, and the secondary stream was supplied at four subsonic Mach numbers from nozzles of variable area and shape. Coaxial and eccentric nozzle configurations were investigated. In the coaxial arrangements, the secondary flow reduces the growth rate of the primary shear layer and elongates the primary potential core. As a result, the mass entrainment rate of the coaxial jet is less than that of the single jet. The potential core is stretched by 68% when a secondary stream with area ratio 2.9 is supplied at Mach number 0.9. The eccentric configuration shows substantial improvement in mixing over the coaxial case and achieves an entrainment rate roughly equal to that of the single jet when the exit areas of the primary and secondary streams are approximately equal. On an equal mass flow rate basis, the eccentric dual-stream jet with area ratio 0.9 actually mixes faster than the single jet. The potential core and the supersonic region of the jet are elongated much less than in the coaxial case. A semi-empirical model, based on the present data and classical shear layer relations, is proposed for the primary and secondary core lengths of coaxial jets.

Nomenclature

A	=	cross-sectional area
a	=	speed of sound
D	=	nozzle exit diameter
D_m	=	mass flow rate equivalent diameter [Eq. (5)]
F	=	thrust
H	=	secondary flow thickness
L	=	length of potential core
M	=	Mach number at nozzle exit
M_c	=	convective Mach number
$\dot{m}$	=	mass flow rate
R	=	nozzle exit radius
$\mathcal{R}$	=	velocity ratio across shear layer
r	=	radial coordinate
$\mathcal{S}$	=	density ratio across shear layer
U	=	velocity at nozzle exit
u	=	mean velocity field
$u_{\max}$	=	maximum mean velocity at given axial station
x	=	axial coordinate
α, β	=	fitting constants
δ	=	shear layer thickness
δ'	=	shear layer growth rate, $\mathrm{d}\delta/\mathrm{d}x$
ρ	=	mean density field
ϕ	=	azimuthal angle

Subscripts

coaxial	=	jet with finite annular secondary flow
coflowing	=	jet in an infinite coflow
fast	=	fast stream of shear layer
p	=	primary stream of jet
s	=	secondary stream of jet
single	=	single-stream jet
slow	=	slow stream of shear layer
sp	=	layer between secondary and primary streams
0	=	value at jet exit
∞	=	ambient
∞p	=	layer between ambient and primary stream
∞s	=	layer between ambient and secondary stream

Presented as Paper 2000-2060 at the AIAA/CEAS 6th Aeroacoustic Conference, Lahaina, HI, 12–14 June 2000; received 8 May 2001; revision received 15 November 2001; accepted for publication 21 November 2001.

*Graduate Student, Department of Mechanical and Aerospace Engineering. Member AIAA.
†Professor, Department of Mechanical and Aerospace Engineering. Associate Fellow AIAA.

Introduction

Motivation

THE potential core of a turbulent jet is a region of vital importance to a host of technological applications, including jet engines, fuel injectors, and ejectors. Jet mixing noise is produced mainly around the end of the potential core.[1] Thermal emissions from hot jets scale with the length of the potential core. The effectiveness of ejectors depends on how fast the driver flow mixes with the entrained flow, that is, on how short the potential core can become. In many instances, the jet is surrounded by a secondary flow, as in turbofan engines and coannular fuel injectors. The secondary flow can significantly influence the fluid mechanics of the jet, thereby having an impact on all of the aforementioned applications. The fluid mechanics change, not only because of the reduction in velocity difference, but also because of density and compressibility effects. To date, there are no comprehensive studies that incorporate those effects into physical models for the mean flow development of coaxial jets.

Jet noise is an area of increasing importance as political and environmental pressures for quieter aircraft escalate. Reduction of noise from high-speed jets is a prerequisite for the development of future supersonic transports. For a given exit velocity, the length of the noise source region scales roughly with the length of the potential core. Given that the vast majority of jet engines are coaxial turbofans, many of the unmixed type, the influence of the secondary (fan) flow on the noise source distribution becomes crucial. This influence is particularly noticeable when one uses the secondary flow to prevent noise generation from the primary flow, as in the Mach wave elimination (MWE) technique.[2] In the initial implementations of MWE, the secondary flow was supplied by an annular nozzle around the primary jet. A full-annular secondary flow has the drawback of reducing the spreading rate of the shear layer between the primary and secondary streams. As a result, the primary potential core and, consequently, the noise source region, are stretched considerably. For small annulus thickness (which is desirable to minimize engine cross section) the secondary flow was unable to shield the entire noise source region, hence, the noise reduction was modest.[3] Eccentric arrangements, however, where the inner nozzle is pushed against the inner wall of the outer nozzle, yielded substantial noise reduction in the general direction of maximum secondary

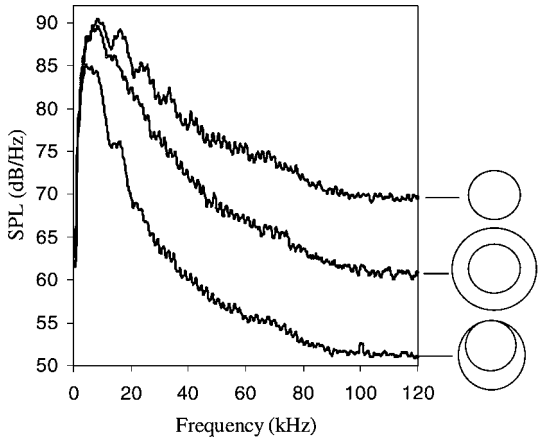

Fig. 1 Far-field sound spectra in the direction of peak emission for single jet ($U_p = 700$ m/s and $M_p = 1.5$) and of the same jet covered by annular and eccentric secondary flows ($U_s = 360$ m/s and $M_s = 1.0$) with same downward thickness.[4]

flow thickness.[4] Centerline pitot surveys showed that the eccentric secondary stream did not significantly elongate the primary potential core. The secondary flow was, thus, able to shield most, if not all, of the noise source region, yielding noise suppression vastly superior to the coaxial case, even when the annulus thickness of the coaxial nozzle and the maximum meniscus thickness of the eccentric nozzle were equal.

Figure 1 compares noise spectra from a single jet and from the same jet covered by annular and eccentric secondary flows, with equal secondary flow thickness in the downward direction. The primary jet was at Mach 1.5 and velocity of 700 m/s, and the secondary stream was at Mach 1.0 and velocity of 360 m/s. The noise measurements were obtained at a distance of 80 jet diameters and angle of 40 deg relative to the jet axis, which is the direction of peak noise emission of the untreated jet. At a frequency of 100 kHz (which, scaled to an aircraft engine, corresponds to 1000–2000 Hz, a range weighed heavily in perceived noise metrics) the asymmetric configuration reduced noise by 19 dB, whereas the symmetric one reduced it by only 9 dB. Furthermore, the eccentric arrangement practically eliminated crackle, a noise source associated with Mach wave emission,[5] whereas the coaxial configuration reduced it only moderately. The full-scale perceived noise of the eccentric jet was less than that of the coaxial jet or the fully mixed equivalent jet. Further details of the acoustics of eccentric jets can be found in Ref. 4. It is surmised, therefore, that the advantage of the eccentric arrangement is due to its shorter potential core relative to the coaxial jet. The example cited here underscores the need for better understanding of the mean flow characteristics of dual-stream jets.

Early works on coaxial jets were motivated mainly by applications in combustion and aircraft propulsion. Several studies in subsonic, axisymmetric, turbulent coaxial jets have investigated the development of the flowfield in the near-field region and its approach to a self-preserving state.[6–10] The overall conclusion from these studies is that the flow development is affected by the velocity and density ratios across the shear layers, as well as the area ratio between primary and secondary streams. There are scarce experimental data, however, on potential core lengths of either the primary or secondary flows. Perhaps the first well-documented study of coaxial jets is that of Forstall and Shapiro.[6] They examined the mass and momentum transfer in a low-speed jet surrounded by the airstream of a wind tunnel. In our nomenclature, we call this a coflowing jet, that is, a jet surrounded by a very large secondary flow. Forstall and Shapiro determined that the spreading rate and turbulent transport are governed by the velocity ratio $\mathcal{R} = U_s/U_p$. Williams et al.[7] investigated the flow structure and acoustics of cold, subsonic, compressible coaxial jets and suggested empirical relations for their primary potential core length and their noise emission. The effects of density ratio and compressibility, which we now know are significant, were absent from their correlations. Champagne and Wygnanski[8] investigated low-speed coaxial jets emerging from a planar wall. It was determined that the primary core length increases with velocity ratio and with secondary-to-primary area ratio. The reported potential core lengths, however, are much higher than those of other studies, even in the case of the single jet. For example, the potential core length of their single jet is 7.5 diameters long, whereas the typical value found in the literature is 4 diameters.[11,12] This is undoubtedly due to the presence of the planar wall, which reduces the entrainment rate of the jet relative to a jet unobstructed by any solid boundaries. Ko and Kwan[10] obtained mean velocity profiles in the initial region of incompressible coaxial jets and identified three distinct regions: the initial merging zone where both the primary and secondary potential cores are found, the intermediate zone between the end of the secondary potential core and the end of the primary potential core, and the fully merged zone. Similarity of the mean velocity and turbulent-intensity profiles within the two shear layer regions of the initial zone, and within the fully merged zone, was observed. No similarity was obtained in the intermediate zone. It was found that the primary and secondary potential cores are both elongated as the velocity ratio is increased.

Only a handful of investigations have encompassed coaxial jets with supersonic primary flow. Eggers and Torrence[13] obtained data on turbulent mixing for supersonic coaxial air jets with inverted velocity profiles ($U_s/U_p > 1$). Schadow et al.[14] conducted spreading rate measurements in supersonic coflowing jets with normal velocity profile and determined that the effect of compressibility on the growth rate is very similar to that measured in planar shear layers. Recently, Cutler et al.[15] investigated a supersonic coaxial jet with a primary flow composed primarily of helium and a secondary flow composed of air. One of their conclusions was that the spreading rate of the primary shear layer was close to that predicted by planar shear layer models. Dahl and Morris[16,17] used linear stability analysis to predict the noise radiated from instability waves in coaxial jets with normal and inverted velocity profiles. Because of the lack of mean flow data, they found it necessary to calculate the mean velocity field using a mixing length model.[18] It is clear that benchmark data on coaxial supersonic jets are needed to increase our understanding of the flow phenomena that govern mixing and noise generation. Although the aforementioned works provide useful insights, there has been no systematic study on the effects of velocity, Mach number, and area ratio of the secondary flow on the mean flow development of supersonic dual-stream jets.

The primary objective of our study is to develop scaling laws for the potential core region of single- and dual-stream, high-speed jets. It was deemed important to include not only the conventional coaxial arrangement, but also the eccentric arrangement that proved so beneficial in reducing Mach wave emission (Fig. 1). We chose cold air jets because of the ease by which one can compute velocity and density profiles from pitot pressure surveys. However, the models proposed here are general enough to be used with hot or variable-composition jets.

Planar Shear Layer Model

The near field of a dual-stream jet consists of two shear layers, one between the primary and secondary flows, and the other between the secondary flow and the ambient air, as illustrated in Fig. 2.

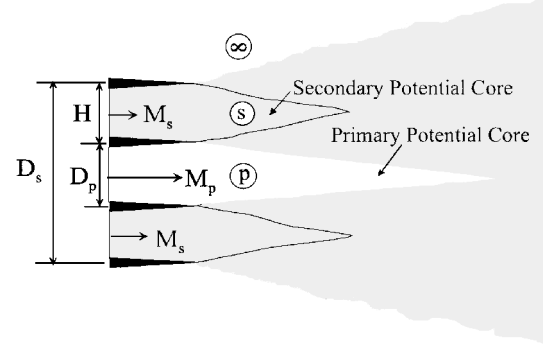

Fig. 2 Principal features of coaxial jet flow.

Each shear layer is similar to a planar shear layer as long as its thickness is small compared to the radius of the potential core that it surrounds.[19] It is, thus, important to review the planar shear layer relations because they will prove helpful in developing models for the potential core lengths of the coaxial jet.

It is important to realize, however, that the classical shear layer relations can be used quantitatively only in the case of a single jet or a jet surrounded by a very large coflowing medium. In both instances, the shear layer is formed between clean, well-defined freestream conditions. This is not the case in the coaxial jet with finite thickness secondary flow. The stream surrounding the primary shear layer is bounded by another shear layer, the secondary one, that exhibits instability and growth. When the secondary core ends, the primary shear layer is exposed to rapidly changing freestream conditions on its outer side. The secondary shear layer is not clean either because it is bounded by the unstable primary shear layer. Nevertheless, we will see that, for the purpose of modeling the potential core length, the coaxial jet can be treated as an intermediate flow between the single jet and the coflowing jet. The classical shear layer models will help us determine the end points of this relation.

When a compressible shear layer between a fast and a slow stream is considered, its growth rate can be expressed as[20]

$$\delta' = \delta'_{\text{inc}}(\mathcal{R}, \mathcal{S}) f(M_c) \tag{1}$$

where

$$\delta'_{\text{inc}} = C\frac{(1-\mathcal{R})\left(1+\sqrt{\mathcal{S}}\right)}{1+\mathcal{R}\sqrt{\mathcal{S}}} \tag{2}$$

is the growth rate of the equivalent incompressible shear layer, with $\mathcal{R} = U_{\text{slow}}/U_{\text{fast}}$, $\mathcal{S} = \rho_{\text{slow}}/\rho_{\text{fast}}$, and C a constant that depends on the definition of layer thickness. Here, $f(M_c)$ is a compressibility correction based on the convective Mach number

$$M_c = \frac{U_{\text{fast}} - U_{\text{slow}}}{a_{\text{fast}} + a_{\text{slow}}} \tag{3}$$

A curve fit through the growth rate data of various investigations[20–23] gives the approximation

$$\delta'/\delta'_{\text{inc}} = f(M_c) = 0.23 + 0.77\exp\left(-3.5M_c^2\right) \tag{4}$$

which describes the stabilizing effect of convective Mach number on the growth rate. For the growth rate of the pitot thickness, which is the width of the pitot pressure profile from 5 to 95% of the difference in the freestream values, Papamoschou and Roshko[20] determined the constant in Eq. (2) to be $C = 0.14$.

Experimental Program

Experiments were conducted in the dual-stream jet facility depicted in Fig. 3 and described in several earlier publications.[2,4] Coaxial and and eccentric nozzle configurations were derived from the same nozzle assembly. Air at room temperature was supplied to the primary and secondary nozzles. The primary (inner) nozzle had an inner exit diameter $D_p = 12.7$ mm and was designed by the method of characteristics for Mach number $M_p = 1.5$. The outer exit diameter of the inner nozzle was 13.4 mm. The jet Reynolds number was 5.5×10^5. Three conical secondary (outer) nozzles were used, with exit diameters $D_s = 17.8$, 21.6, and 25.4 mm. The primary jet was perfectly expanded and the surrounding air was at ambient, still conditions. The secondary flow was naturally pressure matched at subsonic conditions. Nozzle configurations and flow conditions are summarized in Tables 1 and 2. For ease of reference, we use a labeling system that describes the size and shape of the secondary nozzle and the Mach number of the secondary flow. Coaxial nozzles are denoted by Cxx and eccentric nozzles by Exx, where $xx = 10 \times D_s/D_p$. The secondary flow is denoted by Myy, where $yy = 100 \times M_s$. Case C20M37, for example, describes the coaxial jet with Mach 0.37 secondary flow exhausting from a coaxial arrangement with $D_s/D_p = 2.0$. Case E17M90 has a Mach 0.9 secondary stream supplied through an eccentric configuration with $D_s/D_p = 1.7$. The single Mach 1.5 jet is denoted single.

Table 1 Nozzle configurations

Nozzle	D_s/D_p	A_s/A_p	Configuration
C14	1.4	0.9	Coaxial
C17	1.7	1.8	Coaxial
C20	2.0	2.9	Coaxial
E14	1.4	0.9	Eccentric
E17	1.7	1.8	Eccentric

Table 2 Flow conditions

Case	M_p	U_p, m/s	ρ_p/ρ_∞	M_s	U_s, m/s	ρ_s/ρ_∞
Single	1.5	430	1.45	0	0	1.00
M37	1.5	430	1.45	0.37	130	1.03
M60	1.5	430	1.45	0.60	210	1.07
M90	1.5	430	1.45	0.90	290	1.16

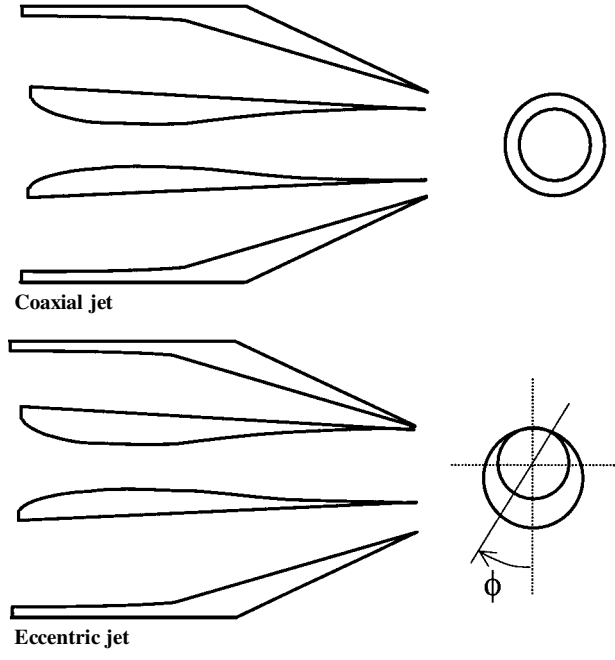

Fig. 3 Nozzle configurations used in present study; diameter of the primary jet was 12.7 mm.

Pitot probe surveys were conducted at various downstream positions from the jet exit. The inlet of the pitot tube was flattened to an opening of 0.2×2.0 mm, thus giving a spatial resolution of about 0.2 mm. The probe was mounted on a carriage that traversed the jet plume at a controlled speed that ranged from 6 to 14 mm/s. The probe was connected to a pressure transducer (Setra Model 280), also mounted on the carriage to minimize the length of tubing between the probe and the transducer. Extensive testing showed that the response time of the probe–transducer system was low enough to resolve the sharp gradients in pitot pressure near the nozzle exit at the traversing velocities mentioned. Mach number, velocity, and density profiles were computed from the pitot pressure profiles under the assumptions of constant static pressure (equal to ambient value) and constant total temperature (equal to room temperature). Radial profiles of pitot pressure were obtained at streamwise locations from $x/D_p = 0$ to 20 at increments of $x/D_p = 1$. For cases in which a short secondary potential core was expected, particularly with nozzle C14, profiles in the near field of the jet were obtained at finer increments of $x/D_p = 0.25$. For the coaxial jets, it was sufficient to obtain profiles on a single plane passing through the jet axis. For the eccentric configurations, profiles were obtained on the azimuthal planes $\phi = 0$, 23, 45, 68, and 90 deg. These intervals were fine enough to allow accurate interpolation for intermediate values of ϕ and, thus, to obtain the entire jet flowfield.

Development of scaling laws for coaxial jets is more complicated than for single jets. The question is how one normalizes the axial

Table 3 Mass flow rate and thrust ratios

Case	$\dot{m}_s/\dot{m}_p$	F_s/F_p	D_m/D_p
C14M37, E14M37	0.20	0.06	1.10
C14M60, E14M60	0.33	0.15	1.15
C14M90, E14M90	0.52	0.35	1.23
C17M37, E17M40	0.39	0.11	1.18
C17M60, E17M60	0.65	0.30	1.28
C17M90, E17M90	1.02	0.69	1.42
C20M37	0.62	0.18	1.27
C20M60	1.03	0.48	1.42
C20M90	1.62	1.09	1.62

distance to present data in a unified, consistent fashion. The answer is not universal and depends on the ultimate goals and applications of the study. The complication arises from the fact that, as the secondary Mach number increases, so do the the mass flow rate $\dot{m}$ and the momentum flux (thrust) F of the combined flow. Using the primary flow diameter D_p for normalization means that the comparisons will, in general, be at variable $\dot{m}$ and F. This is useful in applications where the size of the primary jet is constrained and one wishes to determine the effect of secondary stream on the mean flow. When there is some freedom in selecting the sizes, shapes, and conditions of the primary and secondary streams, it may be desirable to compare flows at either constant $\dot{m}$ or constant F. The former comparison is more suitable to the near field, whereas the latter one applies to the far field where the details of the origin are forgotten. Because this study is concerned mainly with the near-field region, we use the mass flow rate equivalent diameter[24]

$$D_m = D_p\sqrt{(\dot{m}_p + \dot{m}_s)/\dot{m}_p} \tag{5}$$

which references all of the jets to the same mass flow rate. Table 3 lists the mass flow ratios, thrust ratios, and D_m/D_p ratios for all of the jets covered in this study.

Results and Discussion

Mean Flow Characteristics

Figure 4 presents the evolution of velocity profiles for the single jet, coaxial jet case C17M90, and eccentric jet case E17M90. The primary and secondary potential cores are outlined with dashed lines. The length of the primary potential core, L_p, is defined as the distance from the jet exit to the axial location where the centerline velocity decays to 90% of the primary exit velocity. A similar definition is not possible for the secondary core because the velocity along its "centerline," $r = (R_p + R_s)/2$, may decrease or increase with downstream distance, depending on the velocity ratio U_s/U_p. Instead, we use the observation that along that centerline the slope of the velocity profile $\mathrm{d}u/\mathrm{d}r$ is zero in the potential core region and negative downstream. We then define the length of the secondary potential core, L_s, as the axial distance where the normalized velocity slope satisfies

$$\frac{H}{U_s}\frac{\mathrm{d}u}{\mathrm{d}r} = -0.1$$

This definition gives results consistent with the disappearance of the flat portion of the velocity profile of the secondary flow. Table 4 lists the measured potential core lengths and supersonic lengths, to be defined hereafter for all of the cases covered.

The potential core length of the single jet is 9.2 jet diameters, or $L_p/D_p = 9.2$. This is a little less than the value $L_p/D_p = 10.7$ predicted by the empirical correlation of Witze[25] for a single-stream, cold Mach 1.5 jet. The difference may be due to imperfections in the nozzle contour creating weak waves that slightly enhance the shear layer mixing. Addition of an annular secondary flow suppresses the growth rate of the shear layer between the primary and secondary streams. As a result, the primary potential core is elongated significantly. For case C17M90, shown in Fig. 4b, $L_p/D_p = 15.1$. Examination of all of the coaxial cases of this study shows that L_p increases with increasing secondary flow Mach number M_s and increasing secondary nozzle area A_s. When the secondary stream issues from an eccentric nozzle, the results are very different. Figure 4c

Table 4 Potential core lengths and sonic lengths

Case	L_s/D_p	L_p/D_p	L_*/D_p	L_*/L_p
Single	——	9.2	11.3	1.23
C14M37	1.5	10.5	12.4	1.18
C14M60	1.8	11.4	13.5	1.18
C14M90	2.4	12.5	14.8	1.18
C17M37	2.5	11.4	13.4	1.18
C17M60	3.4	13.3	15.6	1.17
C17M90	4.6	15.1	17.4	1.15
C20M37	4.2	12.3	14.5	1.18
C20M60	5.1	13.8	16.4	1.19
C20M90	5.5	15.5	18.5	1.19
E14M37	3.0	9.8	11.5	1.17
E14M60	3.7	9.9	12.0	1.21
E14M90	5.0	10.1	12.0	1.19
E17M37	7.5	10.4	12.2	1.17
E17M60	8.3	10.7	12.7	1.19
E17M90	8.8	10.9	13.0	1.19

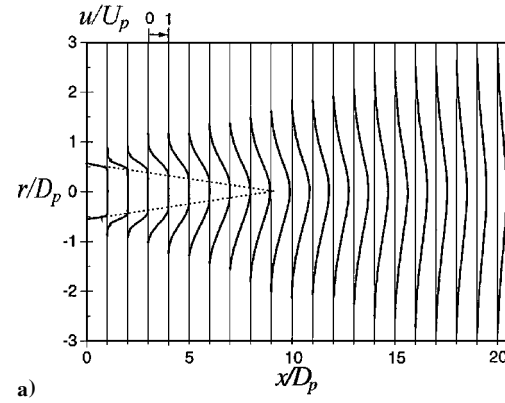

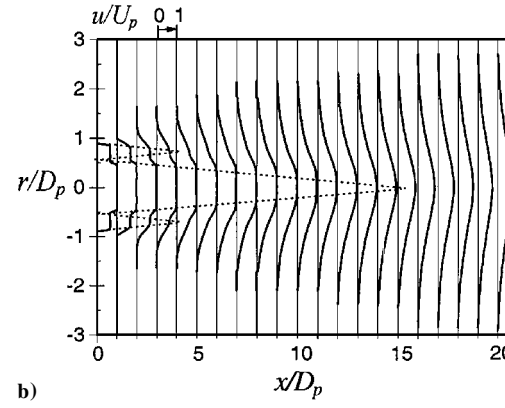

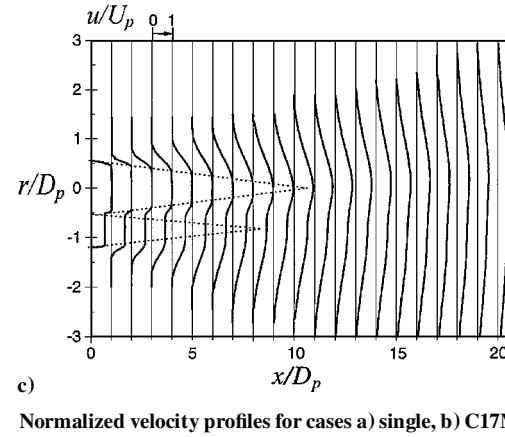

Fig. 4 Normalized velocity profiles for cases a) single, b) C17M90, and c) E17M90.

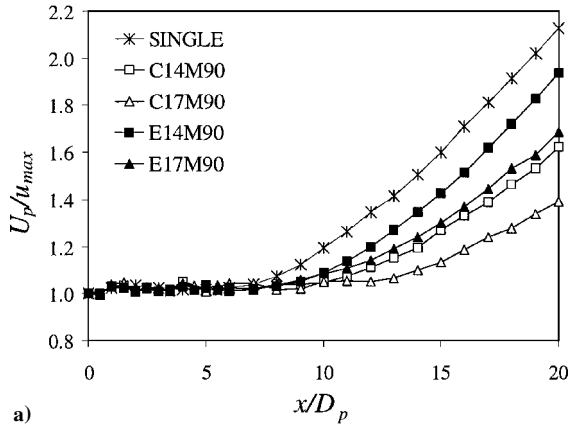

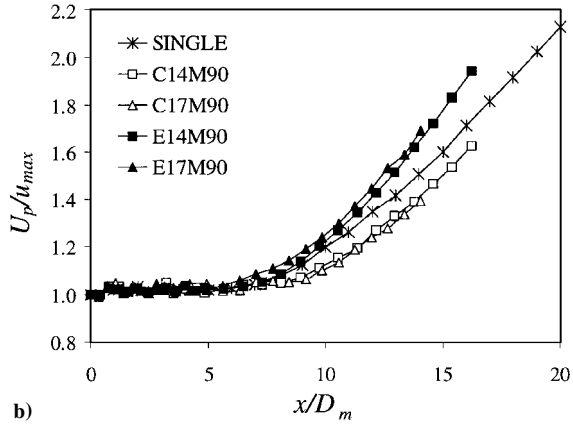

Fig. 5 Inverse of maximum mean velocity normalized by primary exit velocity for jets with Mach 0.9 secondary flow; axial coordinate normalized by a) D_p and b) D_m.

shows velocity profiles surveyed on the azimuthal plane $\phi = 0$ deg of case E17M90, the eccentric counterpart of C17M90. Compared to the coaxial case, the secondary flow on the lower side of the jet has twice the thickness and, thus, has a secondary potential core that is twice as long. The primary potential core length, in this case $L_p/D_p = 10.9$, is much shorter than in the coaxial case and only slightly longer than in the single case.

These observations are quantified further by examining the axial decay of the maximum mean velocity $u_{\max}(x)$. Faster decay indicates more rapid mixing. Figure 5 plots $U_p/u_{\max}$ vs axial position for the single jet and the dual-stream jets with $M_s = 0.9$. The length of the primary core is evident in the plot, as is the development of the jet toward self-similar behavior with increasing axial distance. In Fig. 5a the axial coordinate is normalized by the primary flow diameter. Comparisons at equal thrust and mass flow rate can be made between jets C14M90 and E14M90 and between jets C17M90 and E17M90. It is clear that the eccentric jets have shorter potential core lengths and larger growth rates relative to their coaxial counterparts. All dual-stream jets spread slower than the single jet, with jet E14M90 approaching the growth rate and potential core length of the single jet. Although the jets are not fully developed in the region investigated, progress toward linear growth ($U_p/u_{\max} \sim x/D_p$) is apparent. When the axial coordinate is scaled by D_m (Fig. 5b), the curves for the eccentric jets nearly collapse, as do the curves for the coaxial jets. On an equal mass flow rate basis, the eccentric jets spread faster than the single jet, whereas the coaxial jets spread slower. One should be cautious, however, in characterizing the behavior of the eccentric jets as mixing enhancement. A better explanation is that the two streams of the eccentric jet achieve a certain level of independence from each other. This can be better understood by applying the D_m scaling to a set of multiple, noninteracting jets. The spreading rate of the set increases with increasing number of jets, but there is no mixing enhancement in the sense of greater flow instability.

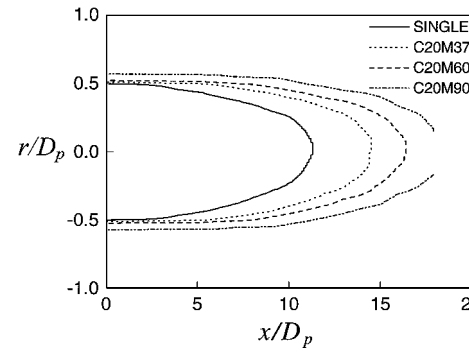

Fig. 6 Sonic lines for coaxial cases with nozzle C20, with comparison to case single jet.

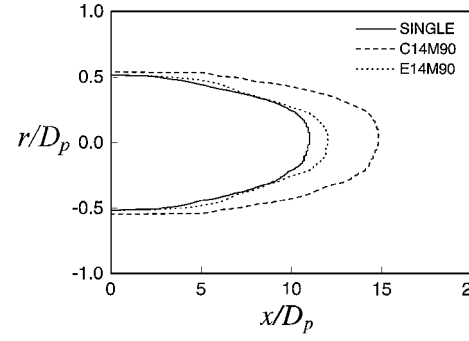

Fig. 7 Sonic lines of jets single, C14M90, and E14M90.

Aside from the potential core, a region of relevance to high-speed jet noise is the extent of the flow that has supersonic motion relative to the ambient, defined by $u/a_\infty > 1$. The supersonic region contains intense noise sources[1] such as Mach waves and, in the case of imperfectly expanded jets, screech/broadband shock noise. To locate the supersonic region we trace the location of the sonic line $u/a_\infty = 1.0$. The length of the supersonic region is denoted L_*. Sonic line contours are plotted in Fig. 6 for coaxial jets with the C20 secondary nozzle. Note that the supersonic region stretches with increasing secondary-flow Mach number. Figure 7 compares the sonic lines of cases single, C14M90, and E14M90. The coaxial jet has a supersonic region 31% longer than that of the single jet. In contrast, the supersonic region of the eccentric jet is only 6% longer. Similar trends are observed in the comparisons of other coaxial and eccentric cases. Comparing the supersonic lengths with the potential core lengths listed in Table 4, we note that the two are roughly proportional, $L_*/L_p \approx 1.2$. This ratio is close to the ratio $U_p/a_\infty = 1.24$, which suggests the relation $L_*/L_p \approx U_p/a_\infty$ for supersonic jets.

Mass Flow Rates

A quantitative measure of mixing is the mass flow rate of the jet plume

$$\dot{m} = \int_A \rho u \, \mathrm{d}A \tag{6}$$

The mass flow rate was calculated from the velocity and density profiles obtained at each downstream station. In theory, integration should be performed over a very large area, at the edge of which the velocity approaches zero. In practice, however, the finite dynamic range of the transducer recording the pitot pressure limits the lower velocity that can be resolved. In our case, the minimum resolvable Mach number was 0.14, corresponding to a transducer dynamic range of 200. Integrating the profiles up to this value creates the inconsistency, however, that the calculated momentum flux varies with axial distance. This is not plausible in a freejet and gives erroneous values for the mass flux. To resolve this issue, we defined the integration area such that the momentum flux at each axial station was 99% of the exit value, that is,

$$\int_A \rho u^2 \, \mathrm{d}A = 0.99F \tag{7}$$

where F is the total thrust computed from the pitot profile at the nozzle exit. For the coaxial jets, the mass flux was computed from

$$\dot{m}(x) = 2\pi \int_0^{R(x)} \rho(x, r) u(x, r) r \, \mathrm{d}r \tag{8}$$

with $R(x)$ defined from

$$0.99F = 2\pi \int_0^{R(x)} \rho(x, r) u^2(x, r) r \, \mathrm{d}r \tag{9}$$

The corresponding calculations for the eccentric jets were more complicated because they entailed integration in both the radial and azimuthal directions. The mass flow rate was given by

$$\dot{m}(x) = 2 \int_0^{\pi} \int_0^{R(x,\phi)} \rho(x, r, \phi) u(x, r, \phi) r \, \mathrm{d}r \, \mathrm{d}\phi \tag{10}$$

where, for fixed $x = x_1$, $R(x_1, \phi)$ describes the isovelocity contour $u[x_1, R(x_1, \phi)] = K(x_1) u_{\max}(x_1)$, with $u_{\max}(x_1)$ the local maximum velocity and $0 < K(x_1) < 1$. The parameter $K(x)$ was set such that the corresponding $R(x, \phi)$ satisfied the invariance of thrust:

$$0.99F = 2 \int_0^{\pi} \int_0^{R(x,\phi)} \rho(x, r, \phi) u^2(x, r, \phi) r \, \mathrm{d}r \, \mathrm{d}\phi \tag{11}$$

The mass flow rate was normalized by the nozzle exit value $\dot{m}_0$ to obtain the entrainment rate of the jet. The entrainment rate was insensitive on the choice of thrust threshold. Thresholds of $0.95F$ and $0.90F$ yielded practically the same results as those presented here using the threshold $0.99F$.

Figure 8 plots $\dot{m}/\dot{m}_0$ vs axial distance for the single jet and for all of the dual-stream jets with the Mach 0.9 secondary flow. In Fig. 8a, the axial distance is normalized by D_p. Note that the eccentric arrangements produce entrainment rates larger than those of the coaxial cases. The entrainment rate of case E14M90 is practically the same as that of case single and exceeds substantially the entrainment rate of its coaxial counterpart, C14M90. Case E17M90 mixes faster than C17M90, but displays a marked departure relative to E14M90. From the nozzle exit up to about $x/D_p = 6$, eccentric cases E14M90 and E17M90 share roughly the same behavior. Downstream of this point, however, E17M90 switches to a lower entrainment rate, whereas the entrainment rate of E14M90 increases. The transition point for E17M90 lies between the end of the secondary potential core and the end of the primary potential core. The reduction in entrainment rate of E17M90 seems to contradict its $u_{\max}(x)$ trend seen in Fig. 5. However, this apparent contradiction is based on the classical, self-similar view of the jet. It is evident that this flow is not close to self similarity. Still, the difference in mass flow rate between E14M90 and E17M90 remains an issue for which we do not yet have a physical explanation. This difference persists when we normalize the axial distance by D_m, as done in Fig. 8b. Although the coaxial jets nearly coincide, the eccentric cases deviate from each other significantly past $x/D_m = 5$. We observe this type of departure between jets E14 and E17 for every secondary flow Mach number.

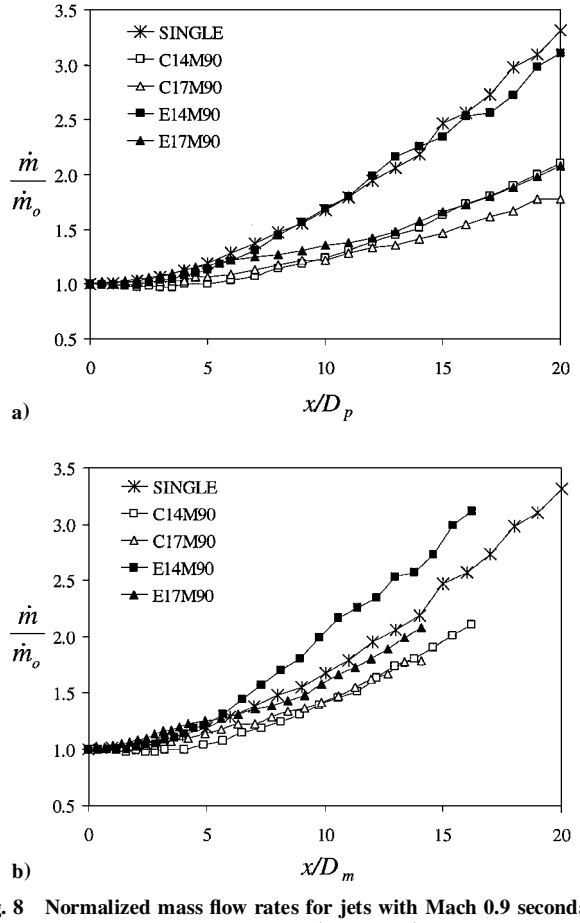

Fig. 8 Normalized mass flow rates for jets with Mach 0.9 secondary flow; axial coordinate normalized by a) D_p and b) D_m.

The linear instability analysis of supersonic coaxial jets by Dahl and Morris[16] may shed some light on the difference in mass flow rates between cases E14 and E17. They found that, when the instability of the primary shear layer dominates, decreasing the area ratio A_s/A_p leads to a rapid increase in the amplification rate of long-wave (low Strouhal number) instabilities near the end of the secondary potential core. One could surmise that, in eccentric jets, the instability of the primary shear layer is always dominant, regardless of the secondary speed. This conjecture is supported somewhat by the fast growth rate of all eccentric jets near the nozzle exit (Fig. 8). Extrapolating Dahl and Morris's findings to eccentric jets, we expect stronger large-scale instability when A_s/A_p is small and reduced instability when A_s/A_p is large, consistent with the trends seen in Fig. 8. Our argument is tenuous and very preliminary at this point. This issue should be addressed by detailed measurements and visualizations of the flow structure in what Ko and Kwan[10] characterized as the intermediate zone of the jet.

Model for the Potential Core Length of Coaxial Jets

In this section we distill our data into models for the lengths of the primary and secondary potential cores of a coaxial jet. We start from two simple, well-defined flows: 1) the single jet and 2) the coflowing jet with primary flow the same as the single jet and surrounded by a very large secondary flow (Figs. 9a and 9b). In both cases, the jet shear layer is surrounded by a flow that is virtually unbounded and with steady, well-defined conditions. Thus, the growth rate should be well approximated by the planar shear layer model. Moreover, the growth rate is expected to be constant from the jet exit to just before the end of the potential core. It is reasonable, therefore, to approximate the potential core length as $L_p/D_p \sim 1/\delta'$ and use the growth rate model described in Eqs. (1–4) to predict δ'. Based on the growth rate and potential core length of case single, the constant of proportionality in the preceding relation is very close to 1.0. Therefore, we write $L_p/D_p = 1.0/\delta'$, where δ' is the pitot thickness growth rate. Specifically, the potential core length of the single jet is

$$L_{\text{single}}/D_p = 1.0/\delta'_{\text{single}}$$

$$= \left\{0.14\left(1 + \sqrt{\mathcal{S}}_{\infty p}\right)\left[0.23 + 0.77\exp\left(-3.5M^2_{c_{\infty p}}\right)\right]\right\}^{-1} \tag{12}$$

where $\mathcal{S}_{\infty p} = \rho_\infty/\rho_p$ and $M_{c\,\infty\,p} = U_p/(a_p + a_\infty)$. The potential core length of the coflowing jet is

$$\frac{L_{\text{coflowing}}}{D_p} = \frac{1.0}{\delta'_{\text{coflowing}}} = \left\{0.14\frac{(1 - \mathcal{R}_{\text{sp}})\left(1 + \sqrt{\mathcal{S}}_{\text{sp}}\right)}{1 + \mathcal{R}_{\text{sp}}\sqrt{\mathcal{R}}_{\text{sp}}}\right.$$

$$\left.\times\left[0.23 + 0.77\exp\left(-3.5M^2_{c_{\text{sp}}}\right)\right]\right\}^{-1} \tag{13}$$

where $\mathcal{R}_{\text{sp}} = U_s/U_p$, $\mathcal{S}_{\text{sp}} = \rho_s/\rho_p$, and $M_{c\text{sp}} = (U_p + U_s)/(a_p + a_s)$.

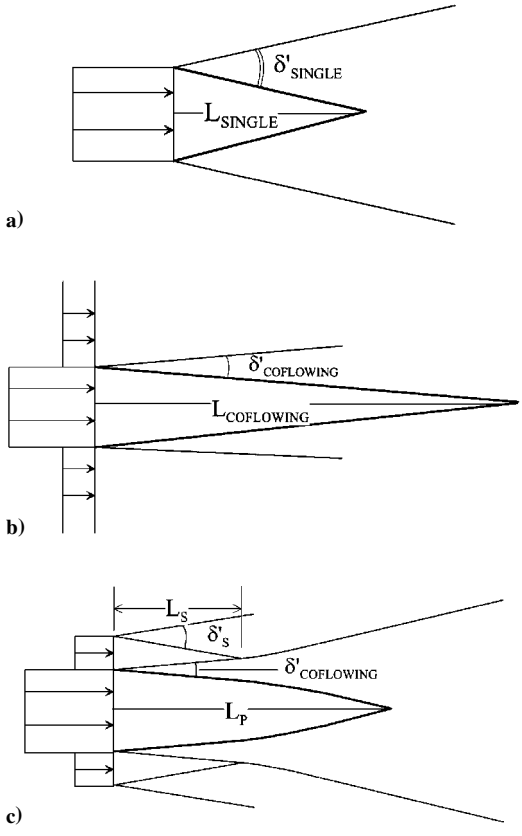

Fig. 9 Potential core development in a) single jet, b) coflowing jet, and c) coaxial jet.

In the coaxial jet (Fig. 9c), the secondary potential core is formed between the outer edge of the primary shear layer and the inner edge of the secondary shear layer. Its length is expected to be inversely proportional to the average growth rate of the surrounding shear layers:

$$L_s/H \sim (\delta'_{\text{coflowing}} + \delta'_s)^{-1} \tag{14}$$

or, using Eq. (13),

$$\frac{L_s}{D_p} = \alpha \frac{H}{D_p}\left[\frac{L_{\text{coflowing}}/D_p}{\delta'_s L_{\text{coflowing}}/D_p + 1}\right] \tag{15}$$

where α is a constant of proportionality and δ'_s is given by

$$\delta'_s = 0.14\left(1 + \sqrt{\mathcal{S}_{\infty s}}\right)\left[0.23 + 0.77\exp\left(-3.5M^2_{c_{\infty s}}\right)\right] \tag{16}$$

with $M_{c_{\infty s}} = U_s/(a_s + a_\infty)$ and $\mathcal{S}_{\infty s} = \rho_\infty/\rho_s$. The constant α in Eq. (15) was obtained by minimizing the normalized standard deviation of the measured data from the model predictions. This yields $\alpha = 2.8$. Figure 10 plots the measured values of L_s/D_p vs the values predicted by the model of Eq. (15). The model predicts the secondary potential lengths with an accuracy of 5%.

Consider now a coaxial jet with secondary potential core shorter than the primary potential core. Initially, the growth rate of the primary shear layer is close to that of the coflowing jet. After the secondary potential core ends, the growth rate of the primary shear layer gradually approaches that of the shear layer in the single jet. We expect, therefore, that the length of the primary potential core L_p will lie somewhere between L_{single} and $L_{\text{coflowing}}$ by an amount dependent on the length of the secondary potential core L_s. As L_s becomes large and approaches $L_{\text{coflowing}}$, L_p should approach $L_{\text{coflowing}}$. Thus, a model for the length of the primary potential core is given by

$$L_p = L_{\text{single}} + f(L_s/L_{\text{coflowing}})(L_{\text{coflowing}} - L_{\text{single}}) \tag{17}$$

where β is a constant and f is a function that increases asymptotically from $f(0) \to 0$ for $L_s/L_{\text{coflowing}} \to 0$ to $f(\beta) \to 1$ for $L_s/L_{\text{coflowing}} \to 1$. The hyperbolic tangent is a natural choice for this function; thus, we set

$$\frac{L_p}{L_{\text{single}}} = 1 + \tanh\left(\beta \frac{L_s}{L_{\text{coflowing}}}\right)\left(\frac{L_{\text{coflowing}} - L_{\text{single}}}{L_{\text{single}}}\right) \tag{18}$$

where the constant β is chosen so as to minimize the normalized standard deviation of our measured data of L_p/L_{single} from their modeled values. This results in $\beta = 2.8$, for which the accuracy of the model is 8% (based on the normalized standard deviation of the measured values from the predicted values). Figure 11 compares the actual values of L_p/L_{single} vs those predicted by the model of Eq. (18). Included in Fig. 11 are data from the scarce past works on coaxial jets that provide potential core lengths or axial velocity decay.[7,10,15] The model predicts those data with an accuracy of 12%.

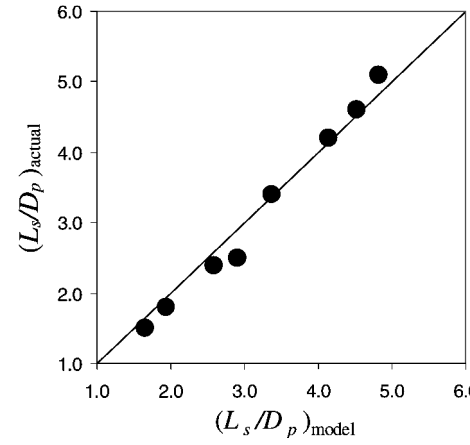

Fig. 10 Measured data of L_s/D_p vs the model predictions of Eq. (15) with fitting constant $\alpha = 2.8$.

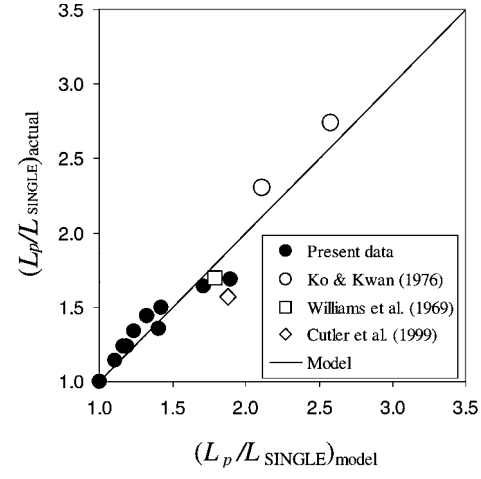

Fig. 11 Measured data of L_p/L_{single} vs the model predictions of Eq. (18) with fitting constant $\beta = 2.8$.

Conclusions

Pitot pressure surveys have characterized the mean flow development of a Mach 1.5 primary jet with secondary flow of variable geometry and Mach number. Coaxial and eccentric configurations were explored. Special attention was placed on the effect of the secondary flow on the potential core lengths, sonic length, and mass flow rate of the jet. In coaxial configurations, the primary potential core is elongated with increasing Mach number and/or increasing area of the secondary flow. For secondary flow at Mach 0.9, delivered from a nozzle with area ratio $A_s/A_p = 2.9$, the potential core is stretched by 68%. The length of the supersonic region of the jet is roughly proportional to the length of the primary potential core

by the factor U_p/a_∞. Thus, the supersonic region is also elongated with the addition of a secondary flow.

The eccentric configuration exposes part of the primary jet to the ambient, thus allowing the jet to grow at a faster rate compared to the coaxial case. As a result, the potential core and sonic lengths are elongated by a much smaller percentage. The normalized mass flow rates of eccentric jets are larger than those of their coaxial counterparts. At area ratio $A_s/A_p = 0.8$, the mass entrainment rate of the eccentric jet with $M_s = 0.9$ practically coincides with that of the single jet. When the jet flows are scaled to equal mass flow rate, the aforementioned eccentric jet actually mixes faster than the single jet. This indicates that the two streams of the eccentric arrangement reach a certain degree of independence from each other. Increasing the area ratio of eccentric jets reduces the entrainment rate in the intermediate region of the jet.

A physical model for predicting the primary and secondary potential core lengths for an arbitrary coaxial jet is proposed. The model combines the present measurements of potential core lengths with classical models of shear layer growth rate. It gives predictions that match reasonably well the present data and those of past works.

Acknowledgments

The support by NASA Langley Research Center is gratefully acknowledged (Grant NAG-1-2104 monitored by Thomas D. Norum). We thank Sky Ellsworth for the construction of the pitot probe traverse system.

References

[1]Bishop, K. A., Ffowcs Williams, J. E., and Smith, W., "On the Noise Sources of the Unsuppressed High-Speed Jet," *Journal of Fluid Mechanics*, Vol. 50, Pt. 1, 1971, pp. 21–31.

[2]Papamoschou, D., "Mach Wave Elimination in Supersonic Jets," *AIAA Journal*, Vol. 35, No. 10, 1997, pp. 1604–1611.

[3]Papamoschou, D., and Debiasi, M., "Noise Measurements in Supersonic Jets Treated with the Mach Wave Elimination Method," *AIAA Journal*, Vol. 37, No. 2, 1999, pp. 154–160.

[4]Papamoschou, D., and Debiasi, M., "Directional Suppression of Noise from a High-Speed Jet," *AIAA Journal*, Vol. 39, No. 3, 2001, pp. 380–387.

[5]Ffowcs Williams, J. E., Simson, J., and Virchis, V. J., "Crackle: An Annoying Component of Jet Noise," *Journal of Fluid Mechanics*, Vol. 71, Pt. 2, 1975, pp. 251–271.

[6]Forstall, W., Jr., and Shapiro, A. H., "Momentum and Mass Transfer in Coaxial Gas Jets," *Journal of Applied Mechanics*, Vol. 10, 1950, pp. 399–408.

[7]Williams, T. J., Ali, M. R. M. H., and Anderson, J. S., "Noise and Flow Characteristics of Coaxial Jets," *Journal of Mechanical Engineering Science*, Vol. 11, No. 2, 1969, pp. 133–142.

[8]Champagne, F. H., and Wygnanski, I. J., "An Experimental Investigation of Coaxial Turbulent Jets," *International Journal of Heat and Mass Transfer*, Vol. 14, No. 9, 1971, pp. 1445–1464.

[9]Durao, D., and Whitelaw, J. H., "Turbulent Mixing in the Developing Region of Coaxial Jets," *Journal of Fluids Engineering*, Vol. 95, No. 3, 1973, pp. 467–473.

[10]Ko, N. W. M., and Kwan, A. S. H., "The Initial Region of Subsonic Coaxial Jets," *Journal of Fluid Mechanics*, Vol. 73, Pt. 2, 1976, pp. 305–332.

[11]Boguslawski, L., and Popiel, C. O., "Flow Structure of the Free Round Turbulent Jet in the Initial Region," *Journal of Fluid Mechanics*, Vol. 90, Pt. 3, 1979, pp. 531–539.

[12]Kassab, S. Z., Bakry, A. E., and Warda, H. A., "Laser Anemometry Measurements in an Axisymmetric Turbulent Jet," *Review of Scientific Instruments*, Vol. 67, No. 5, 1996, pp. 1842–1849.

[13]Eggers, J. M., and Torrence, M. G., "An Experimental Investigation of the Mixing of Compressible-Air Jets in a Coaxial Configuration," NASA TN D-5315, 1969.

[14]Schadow, K. C., Gutmark, E., and Wilson, K. J., "Compressible Spreading Rates of Supersonic Coaxial Jets," *Experiments in Fluids*, Vol. 10, No. 2–3, 1990, pp. 161–167.

[15]Cutler, A., Carty, A., Doerner, S., Diskin, G., and Drummond, P., "Supersonic Coaxial Jet Flow Experiment for Computational Fluid Dynamic Code Validation," AIAA Paper 99-3588, June 1999.

[16]Dahl, M. D., and Morris, P. J., "Noise from Supersonic Coaxial Jets, Part 2: Normal Velocity Profile," *Journal of Sound and Vibration*, Vol. 200, No. 5, 1997, pp. 665–699.

[17]Dahl, M. D., and Morris, P. J., "Noise from Supersonic Coaxial Jets, Part 3: Inverted Velocity Profile," *Journal of Sound and Vibration*, Vol. 200, No. 5, 1997, pp. 701–719.

[18]Dahl, M. D., and Morris, P. J., "Noise from Supersonic Coaxial Jets, Part 1: Mean Flow Predictions," *Journal of Sound and Vibration*, Vol. 200, No. 5, 1997, pp. 643–663.

[19]Bradshaw, P., Ferris, D. H., and Johnson, R. F., "Turbulence in the Noise-Producing Region of a Circular Jet," *Journal of Fluid Mechanics*, Vol. 19, 1963, pp. 591–625.

[20]Papamoschou, D., and Roshko, A., "The Compressible Turbulent Shear Layer: An Experimental Study," *Journal of Fluid Mechanics*, Vol. 197, 1988, pp. 453–477.

[21]Goebel, S. G., and Dutton, J. C., "Experimental Study of Compressible Turbulent Mixing Layers," *AIAA Journal*, Vol. 29, No. 4, 1991, pp. 538–546.

[22]Elliott, G. S., Samimy, M., and Arnette, S. A., "The Characteristics and Evolution of Large-Scale Structures in Compressible Mixing Layers," *Physics of Fluids*, Vol. 7, No. 4, 1995, pp. 864–876.

[23]Hall, J. L., Dimotakis, P. E., and Rosemann, H., "Experiments in Nonreacting Compressible Shear Layers," *AIAA Journal*, Vol. 31, No. 12, 1993, pp. 2247–2254.

[24]Zaman, K. B. M. Q., and Papamoschou, D., "Study of Mixing Enhancement Observed with a Coannular Nozzle Configuration," AIAA Paper 2000-0094, Jan. 2000.

[25]Witze, P. O., "Centerline Velocity Decay of Compressible Jet," *AIAA Journal*, Vol. 12, No. 4, 1974, pp. 417–418.

P. J. Morris
Associate Editor